A molecular approach to the synthesis of platinum-decorated mesoporous graphitic carbon nitride as selective CO_2 reduction photocatalyst

Minoo Tasbihi,[a] Fernando Fresno,[b]* Ignacio Álvarez-Prada,[c] Amitava Acharjya,[d] Arne Thomas,[d] Lluís Escriche,[c] Nuria Romero,[c] Xavier Sala,[c] Víctor A. de la Peña O'Shea,[b] Jordi García-Antón[c]**

[a] Department of Chemistry, Technical University Berlin, 10623 Berlin, Germany.

[b] Photoactivated Processes Unit, IMDEA Energy, Avda. Ramón de la Sagra 3, 28935 Móstoles, Madrid, Spain.

[c] Departament de Química, Unitat de Química Inorgànica, Universitat Autònoma de Barcelona, 08193-Bellaterra, Barcelona, Spain.

[d] Institute of Chemistry: Functional Materials, Technische Universität Berlin, 10623 Berlin, Germany.

KEYWORDS: CO_2 photoreduction, platinum, carbon nitride, UV and visible light, nanoparticles.

Abstract

Platinum nanoparticles (Pt-NPs) have been directly synthesized through the organometallic approach onto the surface of mesoporous graphitic carbon nitride (mpg-CN) semiconductor with two different metal loadings. Thorough multi-technique characterization reveals a very good dispersion of nanoparticles with a narrow size distribution centered at ca. 2.5 nm, regardless of the metal loading, and composed primarily of platinum metal with a minor contribution of oxidic surface species. Compared to bare mpg-CN, the Pt-NPs decorated materials show improved charge separation properties upon band gap excitation, ascribed to electron extraction by Pt-NPs from the conduction band of mpg-CN, as demonstrated by time-resolved fluorescence measurements. The so-obtained materials show photocatalytic activity for CO_2 reduction under both UV and visible light irradiation, with improved selectivity towards highly reduced products such as methanol and methane with respect to the bare semiconductor, which leads to the formation of carbon monoxide as the main product. The obtained results shed light on the pathways that determine selectivity in photocatalytic CO_2 conversion, contributing to the development of selective photocatalysts, which is one of the cornerstones in this promising technology for direct solar-to-chemical energy conversion.

1. Introduction

Releasing a considerable amount of CO_2 because of the high consumption of fossil fuels has led to global warming due to enhanced greenhouse effect, which affects the balance of carbon cycle in nature.[1] Based on this concern, it has become vital for chemists to find ways of transforming undesirable CO_2 into useful chemicals.[2] Among various techniques to reduce the emissions of CO_2, photocatalytic CO_2 reduction to fuels and value added products is considered to be one of the most promising solutions to stabilize the concentration of CO_2 in the atmosphere, while at the same time, it is a direct way to convert solar energy into chemical energy.[3],[4],[5] In 1979, Inoue et al.[6] showed that the photocatalytic reduction of CO_2 in aqueous suspensions of semiconductor powders is feasible and, since then, the high efficiency photocatalytic reduction of CO_2 has become one of the biggest challenges for energy researchers.[7]

Different semiconductors such as TiO_2, Ga_2O_3, ZrO_2, CuO, $LaCoO_3$, CdS, GaP, SiC and carbon nitride (CN) have been studied as photocatalysts for CO_2 reduction.[3],[4],[5],[6],[7],[8] Most of these photocatalysts can only absorb UV light, which limits their photocatalytic performance and future practical application, since UV light represents only around 4% of the solar light that reaches the Earth crust.[9] Therefore, visible-light responsive photocatalysts have recently attracted a great research interest, and their development appears as mandatory, particularly for energy applications of photocatalysis.[10]

Graphitic carbon nitride is a very promising material to be applied as a CO_2 reduction photocatalyst due to its interesting combination of properties like facile and cost-effective synthesis, earth-abundance and nontoxic element composition, thermal stability, and band

structure suitable for CO_2 photoreduction, especially under visible light irradiation.[11] Unfortunately, extended light absorption does not necessarily indicate enhanced photocatalytic performance because the sufficient adsorption/activation of reactants and highly efficient charge separation/transfer also play crucial roles.[12] In addition, one of the key challenges in CO_2 conversion technologies, and particularly in photocatalytic CO_2 reduction, is the control over the selectivity of the process among the different possible carbon products, for example CO, HCOOH, CH_3OH, CH_4, to mention only C_1 products.[1],[13],[14] In this respect, and in the particular case of photocatalysis, probably the simplest and most versatile method to tune the photocatalytic selectivity is to load suitable co-catalysts on the surface of semiconductors.[1],[14] Metal nanoparticles can then play a dual role when supported on a semiconductor photocatalyst: on the one hand, they can improve activity by acting as electron transfer centers and catalytically active sites; on the other hand, they can help tune the product selectivity, since different metals have been reported to lead to the formation of different main products.[1],[14],[15] For example, supported noble-metal co-catalysts, and specifically Pt nanoparticles, have been proved to be particularly interesting for CO_2 reduction due to their excellent activity and selectivity.[16] It is important, though, to have a fine control of the morphological and chemical properties of these nanoparticles, as well as to assure their stability under reaction conditions, in order to fully exploit their potential in this challenging application. In this context, the so-called organometallic approach for the synthesis of metallic nanoparticles allows deposition of small nanoparticles with a controlled surface environment, reproducible size and narrow size distribution under mild synthetic conditions.[17,18] Interestingly, Ru-NPs prepared by this methodology have been recently used as nanocatalysts in the photoproduction of H_2 combined with carbon nitride.[19]

In this study, Pt-NPs@mpg-CN photocatalysts with high Pt dispersion and narrow nanoparticle size have been prepared by the organometallic approach with two different Pt loadings. The photocatalytic activity of as-prepared photocatalysts has been investigated towards photocatalytic reduction of CO_2 under UV and visible light irradiation. The relation between the physical-chemical characteristics and photocatalytic activity has been studied in detail.

2. Materials and methods

2.1. Preparation of photocatalysts. All reactions for the synthesis of the materials were carried out using standard Schlenk-line and Fischer–Porter bottle techniques, or in a glovebox (MBRAUN Unilab) under argon atmosphere. In all cases, glassware was pre-dried prior to use. The following chemicals were used as purchased: [$Pt(dba)_3$] from Strem Chemicals and hydrogen (H_2) gas from Abelló Linde (>99.999%). Tetrahydrofuran (THF) and hexane solvents, from Scharlab, were distilled, dried and degassed by using the freeze–pump–thaw method.

2.2. Synthesis of mpg-CN. Mesoporous graphitic carbon nitride (mpg-CN) has been synthesized according to our previous reported procedure.[20],[21] Cyanamide (CA) was used as the carbon nitride source. Briefly, a certain amount of CA was dissolved in 0.01 N HCl (4 g) and ethanol (4 g) and the pH was adjusted to 2 with 1 M HCl solution followed by the addition of required amount of TEOS (tetraethyl orthosilicate) (CA:TEOS = 6:1). The mixture was stirred for 30 min. After evaporation of the solvents, a transparent glassy gel was observed, which was heated to 80 °C for 24 h to complete dryness. The resulting product was then heated to 550 °C for 4 h in an argon atmosphere. To obtain pure carbon nitride the composites are treated with a 4 M NH_4HF_2 solution for 24 h to completely remove all the silica. After that, the samples were

washed with water several times and finally with ethanol and then dried at 80 °C under vacuum overnight.[20],[21]

2.3. Synthesis of Pt-NPs@mpg-CN photocatalyst. 200 mg of mpg-CN were weighed and placed into a Fischer-Porter bottle directly taken from the oven (120 ºC). The reactor was connected to the vacuum line and allowed to cool to room temperature. Then, 16 mL of THF were added. The reactor was placed in the glove box where [$Pt(dba)_3$] was weighed (11.2 mg, 0.012 mmol for Pt-NPs@mpg-CN(H) or 4.5 mg, 0.005 mmol for Pt-NPs@mpg-CN(L)) and added into the reactor. After this step, the bottle was pressurized with 3 bars of H_2. The reaction was left running overnight (16 h) at room temperature and under vigorous magnetic stirring. After that, the H_2 pressure was evacuated and a TEM specimen was prepared by pipetting a small drop of the colloidal dispersion onto a carbon-coated copper grid (400 mesh). The Pt-based nanomaterials were isolated after washing them with hexane and dried under vacuum. As two different concentrations of [$Pt(dba)_3$] were employed, the as-prepared materials were labeled as Pt-NPs@mpg-CN(H) and Pt-NPs@mpg-CN(L), where (H) is for the higher concentration and (L) for the lower concentration of Pt precursor. These two concentrations have been used as a compromise between high metallic concentrations darkening the materials and preventing light from reaching the photoactive material and low metallic concentrations being less catalytically active.[18] Figure 1 shows a scheme of the synthetic procedure for the preparation of the mpg-CN supported Pt nanoparticles.

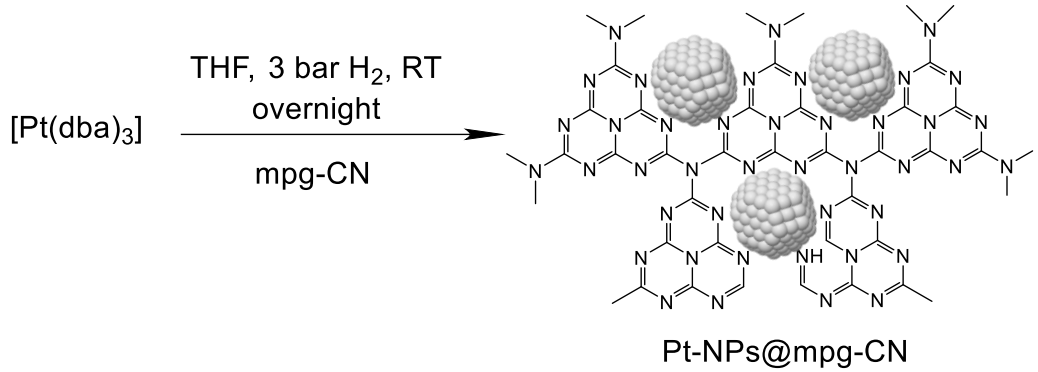

Figure 1. Organometallic approach for the synthesis of the mpg-CN supported Pt nanoparticles.

2.4. Characterization. X-ray diffractograms were recorded in a Panalytical Empyrean diffractometer using Cu K_α radiation at a scanning rate of $0.01°s^{-1}$.

TEM micrographs and EDX spectra were obtained at the Servei de Microscòpia (UAB) with a JEOL JEM 2010 electron microscope working at 200 kV with a resolution point of 2.5 Å. The size distributions were determined via manual analysis of enlarged micrographs, treated with ImageJ software, by measuring ca. 200 particles on several pictures of a given grid to obtain a statistical size distribution and a mean diameter.

The chemical composition of the photocatalysts were investigated using XPS which was performed in an equipment located at Catalan Institute of Nanoscience and Nanotechnology (ICN2) in Barcelona, Spain, with a Phoibos 150 analyzer (SPECS GmbH, Berlin, Germany) in ultra-high vacuum conditions (base pressure $5 \cdot 10^{-10}$ mbar) with a monochromatic aluminum K_α X-ray source (1486.74 eV). The energy resolution measured by the FWHM of the Ag $3d_{5/2}$ peak for a sputtered silver foil was 0.62 eV.

The surface area was measured on a Quantachrome Autosorb-1 apparatus. Nitrogen adsorption–desorption isotherms were measured at 77.3 K after degassing the samples at 120 °C for 6 h. Specific surface areas were determined through the Brunauer-Emmett-Teller (BET) method.

The actual amount of Pt nanoparticles (wt.%) on the semiconductor was measured by an inductively coupled plasma optical emission spectrometry (ICP-OES) Perkin-Elmer Optima 4300DV model system located in the Chemical Analyses Service (UAB), Spain.

UV-vis diffuse reflectance spectra were recorded in a UV/Vis/NIR Perkin Elmer Lambda 1050 spectrometer with a Praying Mantis® diffuse reflectance accessory.

Fluorescence lifetime measurements were carried out by time-correlated single photon counting (TCSPC) with a Mini-τ equipment from Edinburgh Instruments, using as excitation source a pulsed UV laser diode (372.2 nm, 61.2 ps pulse width, repetition rate of 1 MHz) and including a band-pass filter at 450 or ± 25 nm. Experimental data were fitted to bi-exponential decay curves and the average fluorescence lifetime was calculated as $<\tau> = [\Sigma(A_i\tau_i^2)]/\Sigma(A_i\ \tau_i)$, where A_i is the amplitude and τ_i the lifetime of each contribution. Every measurement was performed three times.

2.5. Photocatalytic CO_2 reduction. Gas-phase CO_2 photoreduction experiments were conducted in continuous-flow mode in a stainless-steel reactor with an effective volume of 280 mL and provided with a borosilicate window for irradiation. A suspension of 100 mg of powdered catalyst was deposited on a glass microfiber filter, dried at 100 °C under vacuum and fitted inside the reactor. UV and visible lights are used as irradiation source. In detail, UV illumination was carried out using four 6 W fluorescent lamps with a maximum wavelength at

365 nm and an average irradiance of 71.7 W/m^2 altogether, and visible light irradiation was provided by a 30 W LED white lamp emitting from ca. 400 to 800 nm, with maxima at 445 and 540 nm and with an irradiance of 78.7 W/m^2 reaching the reactor in the full wavelength range. Pure CO_2 and water were fed into the reaction system with a CO_2:H_2O molar ratio of 7.25 using a Controlled Evaporation and Mixing (CEM) unit. The reaction conditions were set at 2 bars and 50 °C. The products of the reaction were determined in-line by a gas chromatograph (GC Bruker 450) equipped with two separation branches and two sampling loops. The first separation branch is equipped with two semicapillary columns (BR-Q Plot and BR-Molesieve5A), a thermal conductivity detector (TCD), a flame ionization detector (FID) and a methanizer. The second separation branch consists of a capillary column (CP-Sil5B) and an FID. Before starting the experiments, the reactor was first evacuated at 50 °C for 1 h and then purged with Ar (100 mL/min) for another 1 h in order to remove any residual organic compounds weakly adsorbed on the surface of the catalyst. Then, CO_2 and H_2O were flowed in the dark for 1 h to establish an adsorption–desorption balance at the reaction temperature. Prior to illumination, the reactor was pressurized and kept at a reaction flow rate of 2 mL/min for another 1 h. A scheme of the reaction system is shown in Figure S1(A). Carbon selectivity was calculated as the cumulative production of every carbon-containing product (i.e., excluding hydrogen) divided by the sum of them. Photonic efficiencies (defined as utilized electrons divided by incident photons in a wavelength interval) were calculated from irradiance measurements taken with a fiber optics spectroradiometer (StellarNet Inc.) and taking into account the different number of electrons necessary to obtain each product from CO_2. ^{13}C isotope tracing experiments were conducted in a 10.8 cm^3 stainless steel reactor provided with a borosilicate top window for irradiation, schematically shown in Figure S1(B). 20 mg of catalyst were deposited from an aqueous

suspension on a glass microfiber filter, dried at 100 °C under vacuum and fitted inside the reactor. After evacuation in vacuum (P < 1 mbar) and 50 °C for 30 min, the reactor was filled with 3 μL of ultrapure water at static vacuum and then with $^{13}CO_2$ (Cambridge Isotope Laboratories, ^{13}C 99%) until a total pressure of 2 bars was reached. The reactor was irradiated in batch mode for 1 h with two 6 W fluorescent lamps (λ_{max} 365 nm), after which the gas was introduced to an Agilent 7820A gas chromatograph equipped with a GS-Carbon-PLOT column and connected to a 5977B mass spectrometry detector with electron impact ionization.

3. Results and discussion

3.1.Characterization of the photocatalysts

The X-ray diffractograms of the synthesized catalysts (Figure 2) show the characteristic reflections of graphitic carbon nitride, with an intense peak at ca. 27.3 º due to the stacking of C_3N_4 layers with an interplanar distance of 0.326 nm, and a weaker one at ca. 13.1º related to inter-planar repetition of triazine units.[22] In addition to these, two new very weak and wide reflections appear in the Pt-NPs@mpg-CN(L) sample that can be indexed as the (111) and (002) planes of the platinum cubic structure, and which become more prominent in the Pt-NPs@mpg-CN(H) sample. In good accordance with TEM images (see below), average Pt particle size calculation by applying the Scherrer equation to the (111) peak in the latter sample diffractogram gives a value of 3.0 nm.

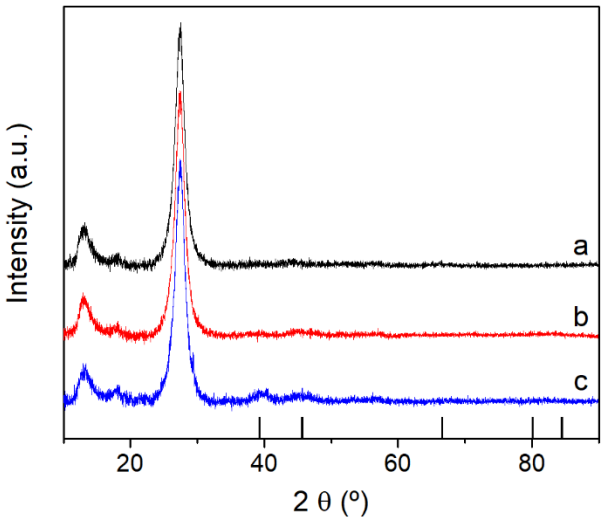

Figure 2. X-ray diffractograms of (a) mpg-CN, (b) Pt-NPs@mpg-CN(L) and (c) Pt-NPs@mpg-CN(H). Black bars indicate the reflections corresponding to the reference Pt structure (ICDD PDF # 01-088-2343).

As it is shown in Figure 3, the TEM images of the as-prepared photocatalysts confirm the presence of small and well-dispersed Pt nanoparticles onto the mpg-CN material. According to the histograms, the mean particle sizes of the Pt nanoparticles are 2.7 ± 0.5 nm and 2.6 ± 0.4 nm for Pt-NPs@mpg-CN(H) and Pt-NPs@mpg-CN(L), respectively.

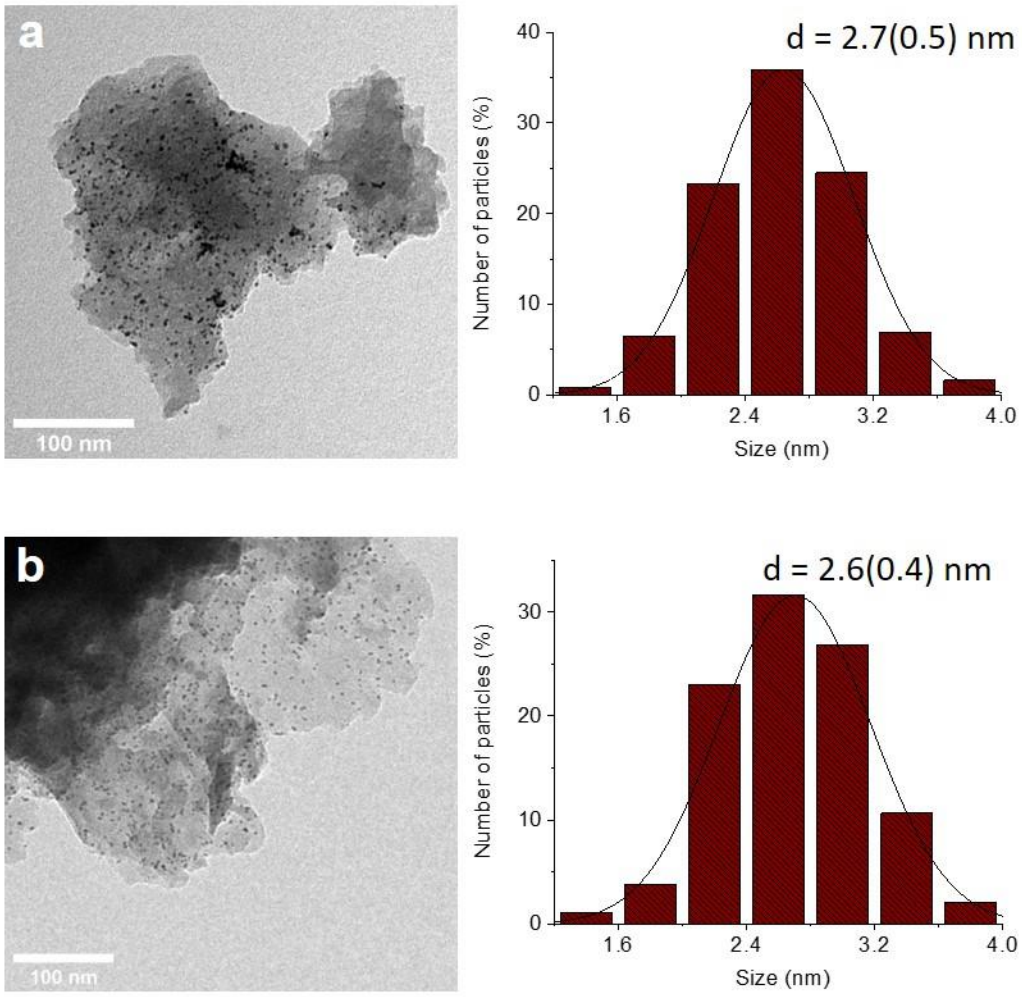

Figure 3. TEM micrographs and size distribution before photocatalytic CO_2 reaction of: a) Pt-NPs@mpg-CN(H) b) Pt-NPs@mpg-CN(L).

These results confirm no significant variation in the mean size of Pt nanoparticles depending on the initial concentration of the Pt precursor, indicating that the difference in XRD patterns is

related to the amount of metal NPs (see below) rather than to their size. This fact, considering the absence of a further stabilizing ligand, demonstrates the effectiveness of the mpg-CN as stabilizing and size-controlling agent for Pt nanoparticles through the organometallic approach. The presence of Pt nanoparticles onto the mpg-CN material was further confirmed by the EDX analyses (Figure S2 in supporting information).

Specific surface areas (S_{BET}) have been measured and studied to find out any possible changes in the structural features of mpg-CN samples (N_2 isotherms can be found in Figure S3). Pure mpg-CN displays a specific surface area of 147.0 m^2/g, which confirms its mesoporosity. After Pt-NPs loading, the specific surface areas of the Pt-NPs@mpg-CN(H) and Pt-NPs@mpg-CN(L) samples decrease to 109.9 (Pt-NPs@mpg-CN(H)) and 114.7 (Pt-NPs@mpg-CN(L)) m^2/g. This behaviour can be attributed to the partial blocking of the mpg-CN mesopores after Pt-NPs loading.

The actual amount of Pt was measured by ICP-OES. 1.2 wt.% Pt and 0.6 wt.% Pt were found for Pt-NPs@mpg-CN(H) and Pt-NPs@mpg-CN(L), respectively, which correspond very well to the nominal Pt values (1.2% and 0.5%) used during the preparation of the hybrid materials.

Additionally, XPS measurements were performed to dig deeper into the chemical nature of the Pt-NPs, both freshly prepared and after being subjected to the photocatalytic experiments detailed in the following section (Figure 4). In all cases, two Pt species have been detected, Pt^0 $4f_{7/2}$ and $4f_{5/2}$ peaks at 70.6 eV and 73.9 eV, and PtO, whose peaks are shifted to 72.9 eV and 76.6 eV compared to the metallic Pt. Previous studies in the literature show that Pt nanoparticles can be partially oxidized.[14]

UV-vis diffuse reflectance spectra (Figure S4 in supporting information) show the typical profile of C_3N_4 semiconductors with a steep absorption onset at ca. 450 nm, corresponding to a band gap of 2.7 - 2.8 eV. The slight apparent variation in the absorption edge observed in the spectra can be probably ascribed to the visible-region baseline caused by the platinum nanoparticles.

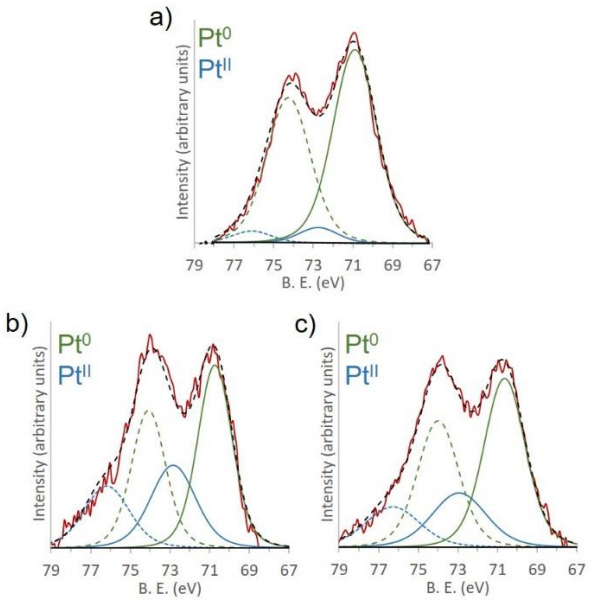

Figure 4. XPS analysis of Pt-NPs@mpg-CN(H) (a) before photocatalytic reaction test (b) after photocatalytic reaction test under UV irradiation (c) after photocatalytic reaction test under visible irradiation. Red lines denote the experimental XPS spectra, dotted black lines the envelope, green lines the metallic-Pt components (Pt 4f), and blue lines the Pt^{II} components (Pt 4f).

Figure 5 shows the fluorescence decay curves obtained with pure and Pt-decorated mpg-CN. The incorporation of the metal nanoparticles induces a reduction of the calculated average fluorescence lifetime, which can be interpreted in terms of electron withdrawal by the metal from the conduction band of the semiconductor upon excitation, reducing the conduction band population and hence decreasing the lifetime of the band-to-band transition involved in

fluorescence.[23],[24] The decrease in the lifetime is larger in the case of the highest platinum content, suggesting the electron transfer occurs to a larger extent with increased amount of nanoparticles.

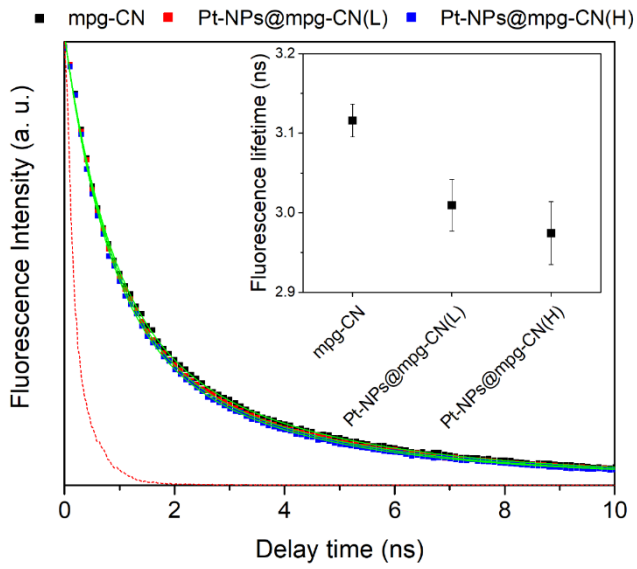

Figure 5. Fluorescence decay curves of bare and Pt-decorated mpg-CN. The green lines correspond to the decay curves fitted to each dataset. The instrument response function (IRF) is represented as a dotted red line. Inset: Average fluorescence lifetimes calculated from the fitted decay curves.

3.2. Photocatalytic reduction of CO_2 under UV and visible irradiation. The developed materials were tested as photocatalysts for gas-phase CO_2 reduction with water as electron donor. As it is shown in Figure 6, CO, CH_3OH, CH_4 and H_2 are detected as the main reaction products under UV light in the presence of the prepared photocatalysts. As could be expected, Pt nanoparticles largely promote the production of hydrogen through the reduction of water competing with that of carbon dioxide.[25] Among carbon products, similarly to previous results with TiO_2,[26],[27]–[28] Pt moves the selectivity from CO to CH_4, and this selectivity is maximum in case of Pt-NPs@mpg-CN(L) photocatalyst. In addition, a significant selectivity

towards CH_3OH is observed with Pt. The maximum methanol selectivity occurs in the presence of Pt-NPs@mpg-CN(H). As seen in Figure 7, where carbon selectivity values are included as defined in the experimental section, this sample shows almost total selectivity towards CH_4 and CH_3OH (ca. 60:40), with CO production practically suppressed. This implies that the selectivity of these catalysts for CO_2 photoreduction under UV light can be, at least, roughly tuned by selecting an appropriate co-catalyst, although further work will be necessary to finely tune the C-product outcome. In this respect, the organometallic approach for the synthesis of metallic nanoparticles is especially relevant since it permits the fine-tuning of the catalytic properties of nanocatalysts through the stabilization of their surface with (limitless) ligands, as done for molecular catalysts.[29],[30]

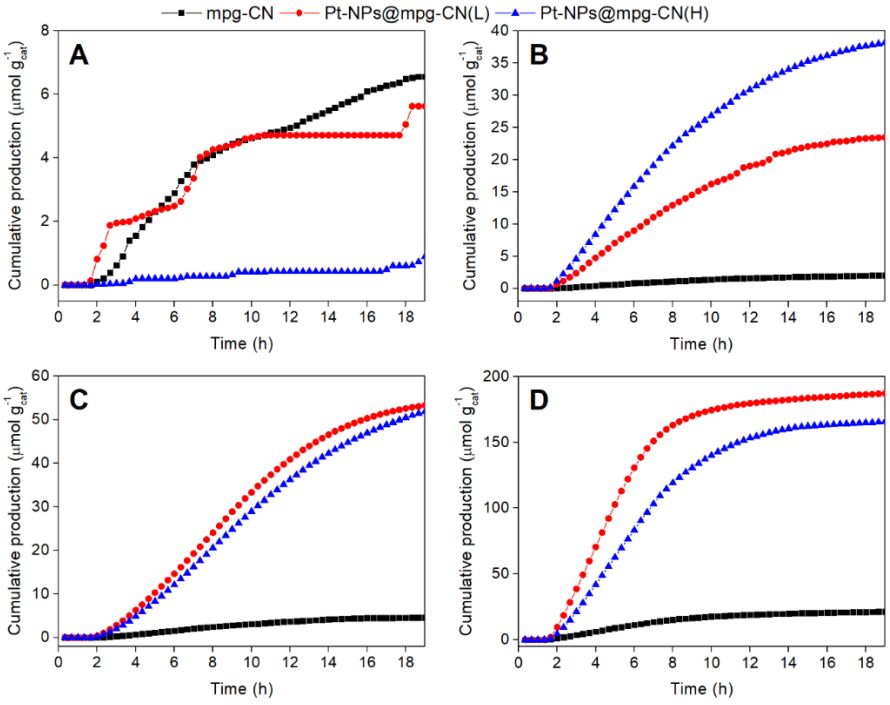

Figure 6. Evolution of the main products obtained in the CO_2 + H_2O photocatalytic reaction under UV irradiation: CO (A), CH_3OH (B), CH_4 (C) and H_2 (D).

As also included in Figure 7, the shift in selectivity when introducing Pt-NPs comes by increased CO_2 conversion and consequently much better electron utilization, both in total terms (C-products and hydrogen outputs) and regarding only electrons transferred into C-products. Thus, from this improved electron utilization, the resulting photonic efficiency between 300 and 400 nm increases in the presence of platinum by one order of magnitude, from ca. 0.003 % in mpg-CN to ca. 0.03% in both Pt-decorated samples.

As outlined in the introduction, however, the most interesting photocatalytic applications of carbon nitride are those carried out under visible light. Figure 8 shows the productions of the main reaction products under visible light irradiation ($\lambda > 400$ nm). On its own, mesoporous graphitic carbon nitride gives rise to the production of mainly CO and H_2, the second one arising from the competitive water reduction reaction, in an approximate ratio 7:1, which means, compared to UV light, a selectivity for CO_2 reduction vs. H_2O reduction much more displaced towards the former. Traces of methanol and methane are also obtained. This product distribution gives rise to a large selectivity of mpg-CN towards carbon monoxide as it is displayed in Figure 7. The presence of Pt nanoparticles promotes the formation of hydrogen, but in a much lower degree than was observed under UV light. This means that a high selectivity for CO_2 reduction vs. H_2O reduction occurs under visible light, which is one of the cornerstones of this reaction.[7] This is illustrated by the values of total electron utilization (C-products + H_2) and electron transfer to C-products displayed in Figure 7, which, unlike the case of UV excitation, are practically equal under visible light. Focusing on carbon products, the presence of platinum nanoparticles clearly displaces the selectivity towards methanol and methane at the expense of CO, and as the amount of Pt increases, the selectivity towards the most reduced product, i.e. CH_4, increases. This might be related to enhanced electron transfer as the number of Pt centers

increases, as suggested by the fluorescence lifetime measurements described above. However, in the presence of Pt-NPs@mpg-CN(H) photocatalyst, the overall CO_2 conversion is considerably lower than that obtained with the Pt-NPs@mpg-CN(L) one, and nearly equals that of the bare carbon nitride. Consequently, the photonic efficiency under visible light (up to 450 nm as correspond to the catalyst absorption spectrum) is maximum with the Pt-NPs@mpg-CN(H) sample with a value of ca. 10^{-2}%. Therefore, there is a clear advantage of the latter catalyst not only in terms of selectivity towards methanol, directly usable as fuel unlike CO, but also in terms of total CO_2 conversion and electron utilization, making this catalyst particularly promising for visible-light CO_2 photoreduction.

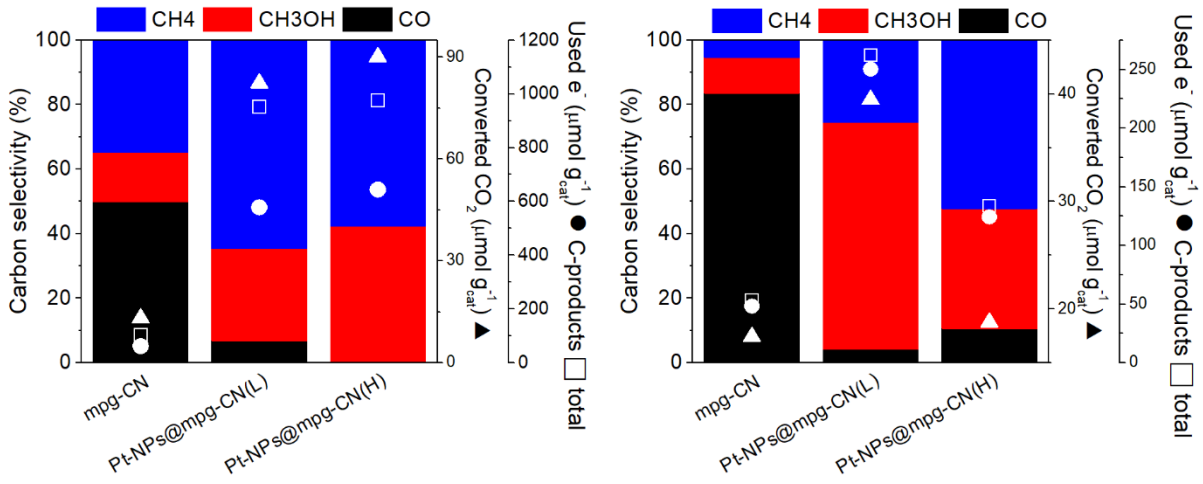

Figure 7. Product selectivities (coloured bars), CO_2 conversions (triangles) and electron use (circles: in C-products; squares: in C-products plus hydrogen) obtained with the different catalysts in the CO_2 + H_2O photocatalytic reaction under UV (left) and visible light (right) irradiation.

It is interesting to note the differences in selectivity observed between UV and visible light reactions. On the one hand, the selectivity towards CO_2 reduction vs. water splitting is much higher under visible light than under UV, even in the presence of a well-known hydrogen

evolution catalyst as Pt. On the other hand, among carbon products visible light excitation appears to favor the formation of methanol vs. that of methane, and indeed the selectivity towards CH_3OH reached by the Pt-NPs@mpg-CN(L) catalyst is as high as 70%. In this respect, it has been reported that excitation with higher photon energy may favor the transfer of a higher number of electrons simultaneously,[31] and this may play a role here in determining whether a more reduced product (CH_4) or a less reduced one (CH_3OH) is formed depending on the excitation wavelength. A similar shift in selectivity has indeed been observed in Ag/TiO_2 photocatalysts when changing from UV to visible light irradiation.[32]

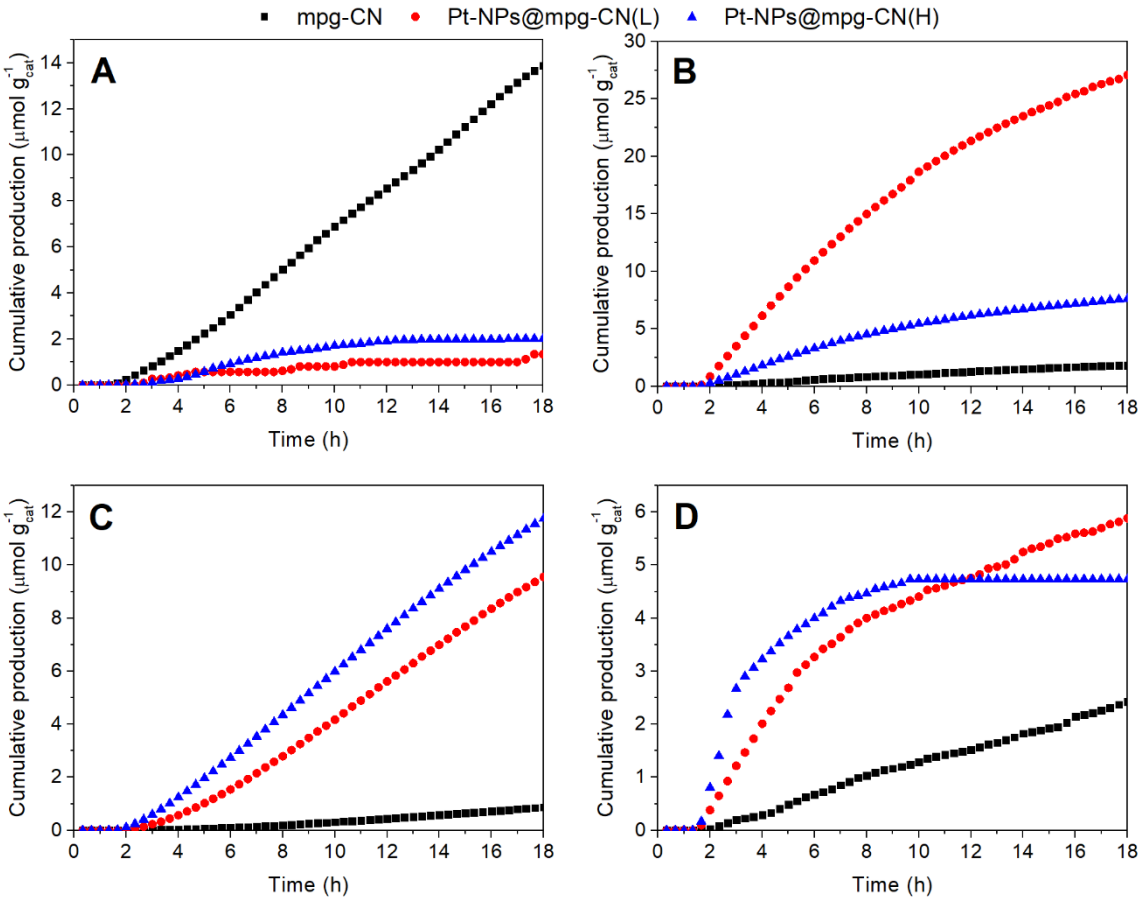

Figure 8. Evolution of the main products obtained in the CO_2 + H_2O photocatalytic reaction under visible irradiation: CO (A), CH_3OH (B), CH_4 (C) and H_2 (D).

Finally, ^{13}C tracing experiments were conducted in order to ascertain the origin of carbon products, by performing a photocatalytic reaction with $^{13}CO_2$ and analyzing the products by GC-MS. The reactor output chromatogram shows a peak at ca. 5 min retention time, whose mass spectrum corresponds to $^{13}CH_4$, as shown in Figure S5 in supporting information, confirming that CO_2 is being reduced to CH_4.

Furthermore, the fate of the catalysts after the photocatalytic experiments were studied by TEM and XPS. The TEM micrographs still show small and well-distributed nanoparticles all over the mpg-CN in all cases (Figure 9), with the presence of Pt confirmed again by EDX analyses (Figure S6 in supporting information). Hardly any variation in size has been observed with respect to the original materials (Table S1 in Supporting Information). XPS spectra after the photocatalytic experiments confirm the chemical stability as observed in Figure 4 b and c.

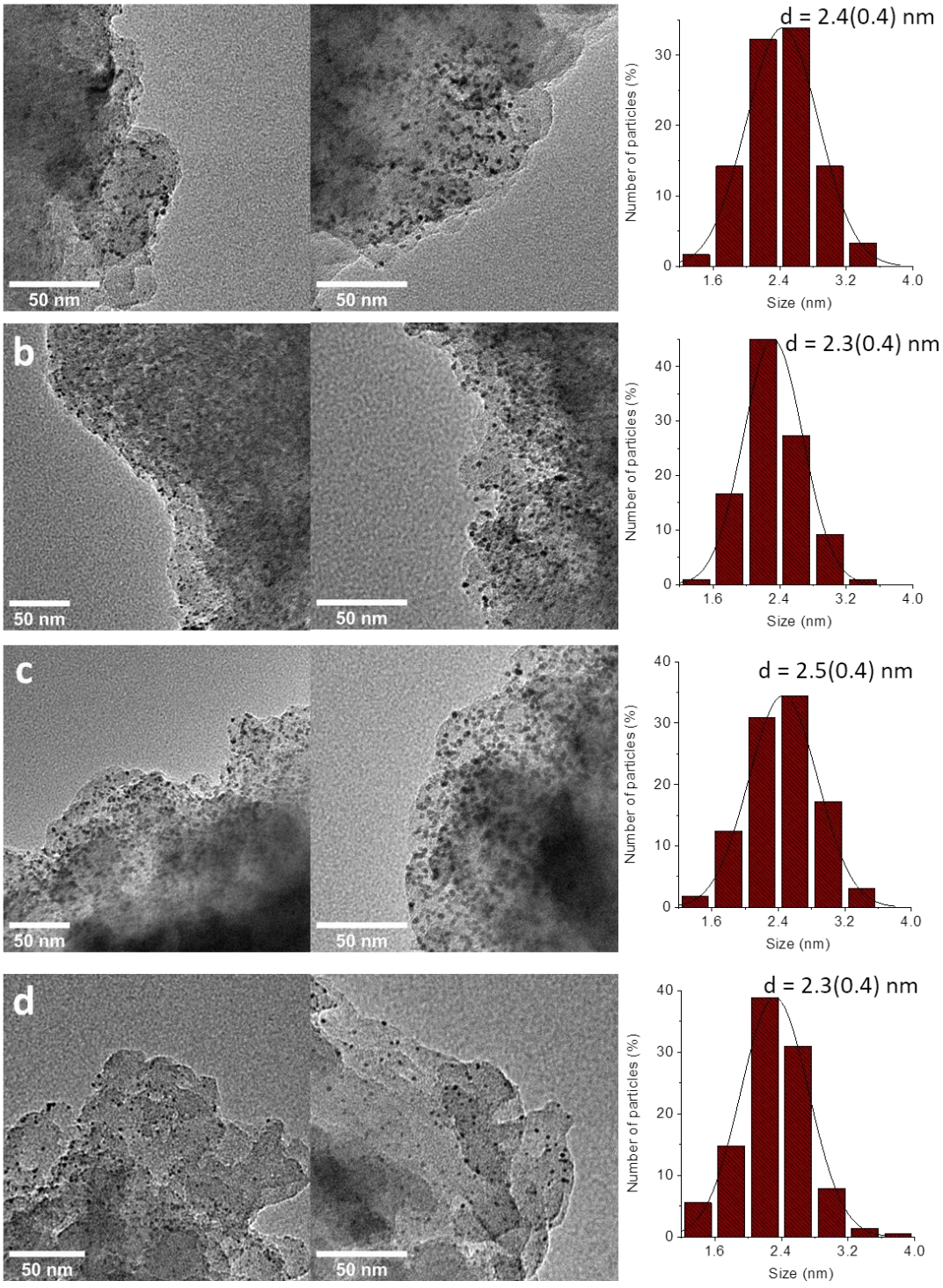

Figure 9. TEM after catalytic reaction. a) Pt-NPs@mpg-CN(H) UV, b) Pt-NPs@mpg-CN(L) UV, c) Pt-NPs@mpg-CN(H) Vis, d) Pt-NPs@mpg-CN(L) Vis.

4. Conclusions

Pt-NPs@mpg-CN photocatalysts have been prepared following the organometallic approach and applied to the reduction of CO_2 in continuous flow reactor under UV and visible light irradiation. Multi-technique characterization reveals a very good dispersion of nanoparticles with a narrow size distribution centered at ca. 2.5 nm, regardless of the metal loading, and composed primarily of platinum metal with a minor contribution of oxidic surface species. Photophysical characterization indicates that electron transfer takes place between the organic semiconductor and the metal nanoparticles. As a result, the so-obtained Pt-decorated mpg-CN shows improved photocatalytic properties in terms of both conversion and selectivity to highly reduced, directly usable fuels such as methanol and methane, with respect to the bare semiconductor, which leads to the formation of carbon monoxide as the main product. The use of the organometallic approach for the synthesis of Pt-NPs has allowed having clean, reproducible and stable surfaces of the nanoparticles, decisive features for the obtaining of the active and selective photocatalysts presented in this work.

Author Statement

M.T., F.F. and J.G.-A. conceived the idea; M.T., F.F., I.A.-P., A.A., A.T., L.E., N.R., X.S., V.A.P.O. and J.G.-A. contributed to experimental design; F.F., I.A.-P., A.A., N.R. and J.G.-A performed the experiments and analyzed data; M.T., F.F., I.A.-P., A.A., A.T., L.E., N.R., X.S., V.A.P.O. and J.G.-A. reviewed the data and prepared the manuscript.

Declaration of competing interest

The authors declare no competing financial interest.

Acknowledgement

The work was supported by the Federal Ministry of Education and Research of Germany through the ”CO2-WIN initiative” under the grant number 033RC024A, by the International Postdoc Initiative (IPODI) of the European Union, by the Spanish Ministry of Science and Innovation (project ENE2017-89170-R, MCIU/AEI/FEDER, EU) and Spanish MINECO (PID2019-104171RB-I00). I. A.-P. acknowledges the Universitat Autònoma de Barcelona for his pre-doctoral grant. J.G.-A. acknowledges Serra Húnter Program. The authors thank the Microscopy Service of the Universitat Autònoma de Barcelona for technical assistance with TEM and SEM.

Appendix A. Supplementary data

Supplementary material related to this article can be found, in the online version, at doi: https://

References

[1] J. Fu, K. Jiang, X. Qiu, J. Yu, M. Liu, Product selectivity of photocatalytic CO2 reduction reactions, Mater. Today. 32 (2020) 222–243. https://doi.org/10.1016/j.mattod.2019.06.009.

[2] G. Centi, E.A. Quadrelli, S. Perathoner, Catalysis for CO2 conversion: a key technology for rapid introduction of renewable energy in the value chain of chemical industries, Energy Environ. Sci. 6 (2013) 1711. https://doi.org/10.1039/c3ee00056g.

[3] Z. Fu, Q. Yang, Z. Liu, F. Chen, F. Yao, T. Xie, Y. Zhong, D. Wang, J. Li, X. Li, G. Zeng, Photocatalytic conversion of carbon dioxide: From products to design the catalysts, J. CO2 Util. 34 (2019) 63–73. https://doi.org/10.1016/j.jcou.2019.05.032.

[4] O. Ola, M.M. Maroto-Valer, Review of material design and reactor engineering on TiO2 photocatalysis for CO2 reduction, J. Photochem. Photobiol. C Photochem. Rev. 24 (2015) 16–42. https://doi.org/10.1016/j.jphotochemrev.2015.06.001.

[5] H. Abdullah, M.M.R. Khan, H.R. Ong, Z. Yaakob, Modified TiO 2 photocatalyst for CO 2 photocatalytic reduction: An overview, J. CO2 Util. 22 (2017) 15–32. https://doi.org/10.1016/j.jcou.2017.08.004.

[6] T. Inoue, A. Fujishima, S. Konishi, K. Honda, Photoelectrocatalytic reduction of carbon dioxide in aqueous suspensions of semiconductor powders [3], Nature. 277 (1979) 637–638. https://doi.org/10.1038/277637a0.

[7] F. Fresno, I.J. Villar-García, L. Collado, E. Alfonso-González, P. Reñones, M. Barawi, V.A. de la Peña O'Shea, Mechanistic View of the Main Current Issues in Photocatalytic CO 2 Reduction, J. Phys. Chem. Lett. 9 (2018) 7192–7204. https://doi.org/10.1021/acs.jpclett.8b02336.

[8] Y. Wang, D. He, H. Chen, D. Wang, Catalysts in electro-, photo- and photoelectrocatalytic CO2 reduction reactions, J. Photochem. Photobiol. C Photochem. Rev. 40 (2019) 117–149. https://doi.org/10.1016/j.jphotochemrev.2019.02.002.

[9] M. Shen, L. Zhang, M. Wang, J. Tian, X. Jin, L. Guo, L. Wang, J. Shi, Carbon-vacancy modified graphitic carbon nitride: enhanced CO 2 photocatalytic reduction performance and mechanism probing, J. Mater. Chem. A. 7 (2019) 1556–1563. https://doi.org/10.1039/C8TA09302D.

[10] M. Melchionna, P. Fornasiero, Updates on the Roadmap for Photocatalysis, ACS Catal. 10 (2020) 5493–5501. https://doi.org/10.1021/acscatal.0c01204.

[11] J. Fu, J. Yu, C. Jiang, B. Cheng, g-C 3 N 4 -Based Heterostructured Photocatalysts, Adv. Energy Mater. 8 (2018) 1701503. https://doi.org/10.1002/aenm.201701503.

[12] S. Cao, Q. Huang, B. Zhu, J. Yu, Trace-level phosphorus and sodium co-doping of g-C 3 N 4 for enhanced photocatalytic H 2 production, J. Power Sources. 351 (2017) 151–159. https://doi.org/10.1016/j.jpowsour.2017.03.089.

[13] R.P. Ye, J. Ding, W. Gong, M.D. Argyle, Q. Zhong, Y. Wang, C.K. Russell, Z. Xu, A.G. Russell, Q. Li, M. Fan, Y.G. Yao, CO2 hydrogenation to high-value products via heterogeneous catalysis, Nat. Commun. 10 (2019) 5698. https://doi.org/10.1038/s41467-019-13638-9.

[14] H. Wang, Y. Wang, Z. Zhu, A. Sapi, K. An, G. Kennedy, W.D. Michalak, G.A. Somorjai, Influence of Size-Induced Oxidation State of Platinum Nanoparticles on Selectivity and Activity in Catalytic Methanol Oxidation in the Gas Phase, Nano Lett. 13 (2013) 2976–2979. https://doi.org/10.1021/nl401568x.

[15] K.S. Bhavani, T. Anusha, P.K. Brahman, Platinum nanoparticles decorated on graphitic carbon nitride-ZIF-67 composite support: An electrocatalyst for the oxidation of butanol

in fuel cell applications, Int. J. Hydrogen Energy. 46 (2021) 9199–9214. https://doi.org/10.1016/j.ijhydene.2021.01.006.

[16] Y. Wang, H. Arandiyan, J. Scott, K.-F. Aguey-Zinsou, R. Amal, Single Atom and Nanoclustered Pt Catalysts for Selective CO 2 Reduction, ACS Appl. Energy Mater. 1 (2018) 6781–6789. https://doi.org/10.1021/acsaem.8b00817.

[17] C. Amiens, D. Ciuculescu-Pradines, K. Philippot, Controlled metal nanostructures: Fertile ground for coordination chemists, Coord. Chem. Rev. 308 (2016) 409–432. https://doi.org/10.1016/j.ccr.2015.07.013.

[18] I. Álvarez-Prada, D. Peral, M. Song, J. Muñoz, N. Romero, L. Escriche, A. Acharjya, A. Thomas, R. Schomäcker, M. Schwarze, X. Sala, M. Tasbihi, J. García-Antón, Ruthenium nanoparticles supported on carbon-based nanoallotropes as co-catalyst to enhance the photocatalytic hydrogen evolution activity of carbon nitride, Renew. Energy. 168 (2021) 668–675. https://doi.org/10.1016/j.renene.2020.12.070.

[19] J. Muñoz, I. Álvarez-Prada, E. Lopez-Lopez, L. Escriche, N. Romero, X. Sala, M. Mas-Torrent, J. García-Antón, Synthesis of 0D to 3D hybrid-carbon nanomaterials carrying platinum(0) nanoparticles: Towards the electrocatalytic determination of methylparabens at ultra-trace levels, Sensors Actuators, B Chem. 305 (2020) 127467. https://doi.org/10.1016/j.snb.2019.127467.

[20] M. Tasbihi, A. Acharjya, A. Thomas, M. Reli, N. AmbroŽová, K. Kočcí, R. Schomäcker, Photocatalytic CO 2 Reduction by Mesoporous Polymeric Carbon Nitride Photocatalysts, J. Nanosci. Nanotechnol. 18 (2018) 5636–5644. https://doi.org/10.1166/jnn.2018.15445.

[21] K. Kailasam, J.D. Epping, A. Thomas, S. Losse, H. Junge, Mesoporous carbon nitride–silica composites by a combined sol–gel/thermal condensation approach and their application as photocatalysts, Energy Environ. Sci. 4 (2011) 4668. https://doi.org/10.1039/c1ee02165f.

[22] A. Thomas, A. Fischer, F. Goettmann, M. Antonietti, J.-O. Müller, R. Schlögl, J.M. Carlsson, Graphitic carbon nitride materials: variation of structure and morphology and their use as metal-free catalysts, J. Mater. Chem. 18 (2008) 4893. https://doi.org/10.1039/b800274f.

[23] U. Noomnarm, R.M. Clegg, Fluorescence lifetimes: fundamentals and interpretations, Photosynth. Res. 101 (2009) 181–194. https://doi.org/10.1007/s11120-009-9457-8.

[24] C.G. López-Calixto, M. Barawi, M. Gomez-Mendoza, F.E. Oropeza, F. Fresno, M. Liras, V.A. De La Penã O'Shea, Hybrids Based on BOPHY-Conjugated Porous Polymers as Photocatalysts for Hydrogen Production: Insight into the Charge Transfer Pathway, ACS Catal. 10 (2020) 9804–9812. https://doi.org/10.1021/acscatal.0c01346.

[25] K. Maeda, K. Domen, Photocatalytic Water Splitting: Recent Progress and Future Challenges, J. Phys. Chem. Lett. 1 (2010) 2655–2661. https://doi.org/10.1021/jz1007966.

[26] M. Tasbihi, F. Fresno, U. Simon, I.J. Villar-García, V. Pérez-Dieste, C. Escudero, V.A. de la Peña O'Shea, On the selectivity of CO2 photoreduction towards CH4 using Pt/TiO2 catalysts supported on mesoporous silica, Appl. Catal. B Environ. 239 (2018) 68–76. https://doi.org/10.1016/j.apcatb.2018.08.003.

[27] J. Ran, M. Jaroniec, S.-Z. Qiao, Cocatalysts in Semiconductor-based Photocatalytic CO 2 Reduction: Achievements, Challenges, and Opportunities, Adv. Mater. 30 (2018) 1704649. https://doi.org/10.1002/adma.201704649.

[28] S. Xie, Y. Wang, Q. Zhang, W. Deng, Y. Wang, MgO- and Pt-Promoted TiO 2 as an Efficient Photocatalyst for the Preferential Reduction of Carbon Dioxide in the Presence of Water, ACS Catal. 4 (2014) 3644–3653. https://doi.org/10.1021/cs500648p.

[29] J. Creus, S. Drouet, S. Suriñach, P. Lecante, V. Collière, R. Poteau, K. Philippot, J. García-Antón, X. Sala, Ligand-Capped Ru Nanoparticles as Efficient Electrocatalyst for the Hydrogen Evolution Reaction, ACS Catal. 8 (2018) 11094–11102. https://doi.org/10.1021/acscatal.8b03053.

[30] J. De Tovar, N. Romero, S.A. Denisov, R. Bofill, C. Gimbert-Suriñach, D. Ciuculescu-Pradines, S. Drouet, A. Llobet, P. Lecante, V. Colliere, Z. Freixa, N. McClenaghan, C. Amiens, J. García-Antón, K. Philippot, X. Sala, Light-driven water oxidation using hybrid photosensitizer-decorated Co3O4 nanoparticles, Mater. Today Energy. 9 (2018) 506–515. https://doi.org/10.1016/j.mtener.2018.07.008.

[31] S. Yu, A.J. Wilson, J. Heo, P.K. Jain, Plasmonic Control of Multi-Electron Transfer and C–C Coupling in Visible-Light-Driven CO 2 Reduction on Au Nanoparticles, Nano Lett. 18 (2018) 2189–2194. https://doi.org/10.1021/acs.nanolett.7b05410.

[32] L. Collado, A. Reynal, F. Fresno, M. Barawi, C. Escudero, V. Perez-Dieste, J.M. Coronado, D.P. Serrano, J.R. Durrant, V.A. de la Peña O'Shea, Unravelling the effect of charge dynamics at the plasmonic metal/semiconductor interface for CO2 photoreduction, Nat. Commun. 9 (2018) 4986. https://doi.org/10.1038/s41467-018-07397-2.